Int J Adv Manuf Technol (2016) 87:3301–3306
DOI 10.1007/s00170-016-8737-7

ORIGINAL ARTICLE

Wear behavior of an Al_2O_3/TiC/TiN micro-nano-composite ceramic cutting tool in high-speed turning of ultra-high-strength steel 300 M

Dong Wang[1] · **Jun Zhao**[2] · **Yan Cao**[1] · **Chao Xue**[1] · **Yu Bai**[1]

Received: 18 December 2015 / Accepted: 4 April 2016 / Published online: 13 April 2016

Abstract An Al_2O_3-based micro-nano-composite ceramic tool material reinforced with TiN micro-particles and TiC nanoparticles was fabricated by using the hot-pressing technique. The wear behavior of the Al_2O_3/TiC/TiN micro-nano-composite ceramic cutting tool (AT10N20) in high-speed turning of ultra-high-strength steel 300 M was investigated by comparison with the commercial Al_2O_3/TiC composite ceramic tool CC650. Worn and fractured surfaces of ceramic cutting tools were observed and analyzed via the scanning electron microscopy (SEM) combined with the energy-dispersive X-ray spectroscopy (EDS). The results showed that the main wear modes of AT10N20 and CC650 were flank wear and rake wear. The crater on the rake face of AT10N20 initially occurred at cutting speed of 400 m/min, while it occurred at cutting speed of 200 m/min for CC650. In addition, the rake wear and flank wear became more severe when the cutting speed attained 400 m/min. The cutting speeds higher than 400 m/min were unfavorable for turning of ultra-high-strength steel 300 M. Wear mechanisms of AT10N20 and CC650 in high-speed turning of the ultra-high-strength steel were abrasion and adhesion.

Keywords Micro-nano-composite ceramic cutting tools · High-speed turning · Wear mechanisms · Ultra-high-strength steel 300 M

✉ Dong Wang
wangdong110104@163.com

[1] School of Mechanical Engineering, Xi'an Technological University, Xi'an 710021, People's Republic of China

[2] Key Laboratory of High Efficiency and Clean Mechanical Manufacture of MOE, School of Mechanical Engineering, Shandong University, Jinan 250061, People's Republic of China

1 Introduction

Ultra-high-strength steels have been widely used in aerospace industries for manufacturing the main structural material of aircraft landing gear due to their attractive mechanical properties such as good stability, high strength, and ductility under high temperature [1, 2]. However, ultra-high-strength steels are known as difficult-to-machine materials, because of their high temperature strength, poor thermal properties, high cutting temperature, severe work hardening, and high tool-workpiece affinity [3–5].

Cemented carbide tools are largely selected to machine ultra-high-strength steels under the relatively low cutting speeds [6–10]. Therefore, cemented carbide tools are unable to meet the requirements of high material removal rate and good surface quality. Ceramic tools are characterized by high hardness, great heat resistance, good wear resistance, and chemical stability [11–15]. They are one of the most important ideal choices in machining ultra-high-strength steels.

Extensive efforts have been made to investigate the tool life, failure modes, and wear mechanisms of mixed ceramic cutting tools during machining of high-strength steels [6, 16–20]. Grzesik et al. [16] explored the wear mechanisms of Al_2O_3/TiC mixed ceramic cutting tools against high-strength steel 5140 in turning operation. The abrasion, plastic flow and transferred layers, fracture, BUE, and tribochemical effects were founded in their cutting experiments. Yan et al. [17] discussed tool wear and chip formation in minimum quantity lubrication milling of high-strength steel PCrNi$_3$Mo. Long et al. [18] studied tribological properties of high-strength steel subjected to HSMS surface modification. Their experiment results indicated that the wear mechanisms of machined surface were grain-abrasion wear, rheological wear, and fatigue wear. These experiments are important for exploring the wear behavior of the ceramic cutting tools in turning of high-strength steels.

In the high-speed turning operation, it is essential to study the tool wear behavior and the effects of cutting parameters on the tool wear mechanisms. In this paper, the Al_2O_3/TiC/TiN micro-nano-composite ceramic cutting tool materials were fabricated by adding micro-scale particle TiN and nanoscale particle TiC into the micro-scale Al_2O_3 matrix. Then, the high-speed turning experiments of 300 M were carried out to investigate the wear behavior of AT10N20 in comparison with the commercial CC650 composite ceramic tools. Worn and fractured surfaces of the ceramic cutting tools were investigated by SEM and EDS to reveal the wear mechanisms.

2 Experimental procedures

2.1 Preparation of Al_2O_3/TiC/TiN micro-nano-composite ceramic tool materials

High-purity micro-scales α-Al_2O_3 particles (purity 99.99 %, Shandong, China), micro-scale TiC particles (purity 99.99 %, Shanghai, China), micro-scale TiN particles (purity 99.99 %, Shanghai, China), and nanoscales TiC particles (purity 99.9 %, Shanghai, China) were used as the starting materials with an average grain size of approximately 0.5, 0.5, 0.5, and 0.14 μm, respectively. The Al_2O_3/TiC/TiN micro-nano-composite ceramic tool materials (AT10N20) were composed of 60 vol% micro-scales α-Al_2O_3 particles, 20 vol% micro-scale TiN particles, 10 vol% micro-scale TiC particles, and 10 vol% nanoscales TiC particles. Firstly, the nanoscale TiC particles were prepared into suspension using alcohol as the dispersing medium, and polyethylene glycol (PEG, Shanghai, China) was used to prevent the aggregation of nanoscale TiC particle after ultrasonic dispersion (with SB5200 ultrasonic instrument and D-7401-III motor stirrer, China) for 15 min. $NH_3{\cdot}H_2O$ was added into the suspension with a pH of 9.0 (with PHS- 25 dogmatic pH- meter, China), and the suspension was dispersed ultrasonically for 20 min. Then, the micro-scale Al_2O_3, TiC, and TiN particles were mixed with the prepared nanoscale TiC particles suspension. Finally, the sintering additives of MgO and NiO powders (Shanghai, China) were added for promoting the densification of the compacts and preventing the grain growth of Al_2O_3 particles during the sintering process. The mixed slurry was ball-milled for 48 h and then was dried in a vacuum dry-type evaporator (Model ZK-82 A, China). After that, the dried powders were sieved through a 200-mech sieve for further use. The dried powders were placed into a graphite die and were hot-pressed with an applied pressure of 32 MPa at 1650 °C for 20 min in a sintering furnace within vacuum atmosphere.

The dimensions of raw sintered ceramic bars were 42 mm in diameter and 10 mm in height. Each sintered ceramics bar was cut off and ground into specimens with the dimensions of 15 mm × 15 mm × 7 mm for the manufacture of cutting tools. Then, the sintered ceramic bars were cut off and polished into specimens with dimensions of 3 mm × 4 mm × 20 mm for the flexural strength test. Flexural strength was measured by using three-point bending method on an electronic universal material testing machine (Model WDW-50E, China) at a loading rate of 0.5 mm/min. Vickers hardness of AT10N20 was measured on the polished specimen surface using a Vickers hardness tester (Model HV-120, China) with a load of 196 N and a holding time of 15 s. The fracture toughness of AT10N20 was calculated via the median crack. At least five specimens were tested to obtain each mechanical property. The properties of AT10N20 are given in Table 1 in comparison with those of commercial CC650 composite ceramic tools, whose properties were obtained from the cutting tool supplier.

2.2 Cutting experiments

The workpiece used in machining tests is an ultra-high-strength steel 300 M bar with 125-mm diameter × 400-mm length. The chemical compositions of ultra-high-strength steel 300 M are listed in Table 2. Two types of ceramic cutting tools were used in experiments. One is Al_2O_3/TiC/TiN ceramic tool AT10N20. Another is commercially available Al_2O_3/TiC ceramic tool CC650 from Sandvik Coromant. Both of the ceramic tools were square-shaped inserts (ISO designation SNGN 120408) and were mounted in a tool holder to offer a rake angle of −5°, clearance angle of 5°, inclination angle of 0°, and side cutting edge angle of 45°.

The high-speed machining tests were performed on a CNC turning center (PUMA200MA) with a maximum spindle speed of 6,000 rpm. All machining tests were implemented with the following cutting parameters: depth-of-cut 0.1 mm, feed rate of 0.1 mm/rev, and cutting speed of 100, 200, 300, 400, and 500 m/min, respectively. During the turning process, the flank wear of the cutting tools was examined periodically using an optical microscope. Mean flank wear value of 0.3 mm was used as the tool wear criterion. Under given conditions, each test was replicated three times. The worn and fractured surface of tools was examined using a SEM (JSM-6380LA, Japan) equipped with an EDS after the experiments.

Table 1 Cutting tool's types, designation, and some properties

Tool material	CC650	AT10N20
Composition	Al_2O_3/TiC	Al_2O_3/TiC/TiN
Type	SNGN 120408T01020	
Vickers hardness (GPa)	21.81	20.8
Flexural strength (MPa)	890	881.4
Fracture toughness (MPa $m^{1/2}$)	5.64	7.8
Young's modulus (GPa)	400	470

Table 2 Chemical compositions of ultra-high-strength steel 300 M (wt%)

Fe	C	Cr	Ni	Mo	Si	V	S	P	Cu
Balance	0.39	0.91	1.82	0.42	1.61	0.07	0.001	0.009	0.06

3 Experimental results and discussions

3.1 Cutting life of wear in Al_2O_3/TiC/TiN micro-nano-composite ceramic tools

Figure 1 shows the cutting lengths of CC650 and AT10N20 at different cutting speeds with fixed feed rate (0.1 mm/r) and depth of cut (0.1 mm) in turning of ultra-high-strength steel 300 M. As can be seen from it, as the cutting speed increases from 100 m/min to 200 m/min, the cutting lengths of both AT10N20 and CC650 become longer. But, with further increase of the cutting speed to 500 m/min, the cutting lengths of both tools decrease gradually. The cutting length reaches its highest value at the cutting speed of 200 m/min; therefore, the speed of 200 m/min is suitable for high-speed turning of ultra-high-strength steel 300 M. The changing trend of cutting length indicates that the ceramic cutting tools are not suitable for cutting ultra-high-strength steel at the low cutting speed (100 m/min). The ceramic tools are sensitive to mechanical shock, and micro cracks and damages are prone to occur during cutting process at relatively low cutting speeds which lead to quick failure of the tool. With the increase of cutting speed, the cutting temperature becomes higher accordingly. The strength and hardness of the ceramic cutting tool could reduce at high temperatures, so the tool life decreases gradually and comes to its lowest value at cutting speed of 500 m/min. The experiment results also show that when the cutting speeds are below 300 m/min, the cutting length of AT10N20 is shorter than that of CC650. CC650 shows better performance than AT10N20. While when the cutting speed speeds are above 300 m/min, the difference of cutting performance between CC650 and AT10N20 reduces. It indicates that AT10N20 is also a good choice for high-speed cutting ultra-high-strength steel 300 M as compared with CC650.

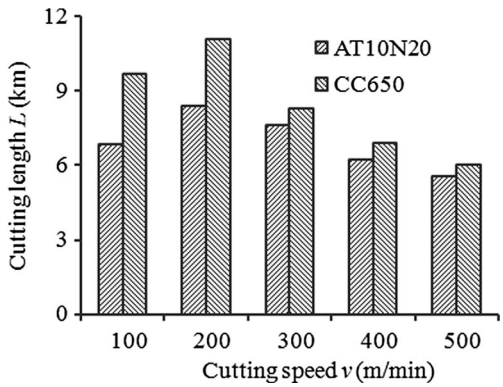

Fig. 1 Cutting lengths of CC650 and AT10N20 at different cutting speeds ($f = 0.1$ mm/r and $a_p = 0.1$ mm)

3.2 Types of wear in Al_2O_3/TiC/TiN micro-nano-composite ceramic tools

Figure 2 shows the SEM micrographs of the AT10N20 ceramic tools in turning of ultra-high-strength steel 300 M at different cutting speeds. The SEM micrographs indicate that the typical types of wear of AT10N20 ceramic tools were flank wear and rake wear. No obvious damages were found on both flank faces and rake faces because of its high strength and toughness. When the cutting speed was less than 300 m/min, the dominant wear mode was flank wear and the slight scratches were found on the rake faces. With the increased cutting speed, the rake wears became serious. When the cutting speed exceeded 300 m/min, the extensive crater wear on the rake faces and nose wear was clearly found.

Figure 3 shows SEM micrographs of the CC650 ceramic tools in turning of ultra-high-strength steel 300 M at different cutting speeds. As shown in Fig. 2, the main wear modes of CC650 ceramic tools were flank wear and rake wear which were the same to those of AT10N20. When the cutting speed was 100 m/min, the dominant wear mode was flank wear and the slight scratches appeared on the rake faces. When the cutting speed exceeded 100 m/min, the extensive wears occurred on the rake face of tools. The crater wear on the rake face became severe as the cutting speed increased.

It is observed from Figs. 2 and 3 that the crater wear on the rake face of AT10N20 initially occurred at cutting speed of 400 m/min, while that of the CC650 occurred at cutting speed of 200 m/min. This difference indicated that the wear resistance of AT10N20 was superior to that of CC650. In addition, the crater wear on the rake faces and flank wear was more severe when cutting speed was 400 m/min which was unfavorable for cutting of ultra-high-strength steel 300 M.

3.3 Wear mechanisms of Al_2O_3/TiC/TiN micro-nano-composite ceramic tools

Ceramic tool wear is generally understood to be caused by mechanical (thermo-dynamic wear, abrasion, and adhesion) and chemical (thermo-chemical wear, diffusion, and oxidation) interactions between the tool and workpiece.

Figure 4 shows SEM micrographs of wear morphology on rake face and flank face of AT10N20 ceramic tools in turning of ultra-high-strength steel 300 M at the cutting speed of 400 m/min. It is clearly seen from Fig. 4 that parallel grooves were regarded as the characteristic of abrasive wear appeared on the rake and flank faces. During turning of ultra-high-strength steel 300 M, the hard inclusions contained in workpiece scratched the flank race along the tool movement direction. The harder particles also scratched the rake face along the

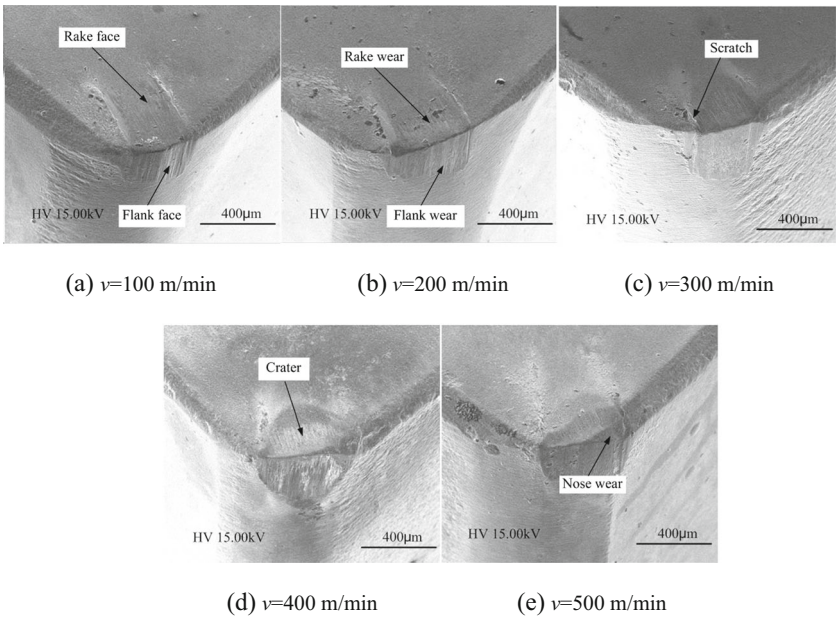

(a) v=100 m/min (b) v=200 m/min (c) v=300 m/min

(d) v=400 m/min (e) v=500 m/min

Fig. 2 SEM of the worn AT10N20 ceramic tools in turning of ultra-high-strength steel 300 M at f = 0.1 mm/r and a_p = 0.1 mm

chip flow direction. The scratching action happened on the tool-workpiece and tool-chip interfaces led to the abrasive wear.

In addition, the adhering layers also generated at the rake face and flank face as shown in Fig. 4. This wear morphology is the typical characteristic of adhesive wear. The adhering layers indicated that the seizure occurred on the interface between the tool and the workpiece. The plastic deformation caused by the high pressure and temperature generated in the high-speed cutting process leads the adhesive wear when the grains of the actual contact area between the tool and the workpiece were fallen off by tension or shear. In high-speed turning of ultra-high-strength steel 300 M, the ceramic tool bears the higher cutting force and thus substantial cutting heat is generated on the region between the tool and the workpiece. However, due to the poor thermal conductivity of ultra-high-strength steel 300 M, the temperature and pressure in the region near the cutting edge will easily reach a high value, the bonding strength between the tool and workpiece material increases rapidly, together with the pore and local defect that exist in the ceramic tool materials, and then the adhesive wear will build and expand.

The wear morphologies on the rake face and flank face of CC650 ceramic tools in turning of ultra-high-strength steel 300 M at the cutting speed of 400 m/min are shown in Fig. 5. Abrasive grooves and adhering layer on the rake face

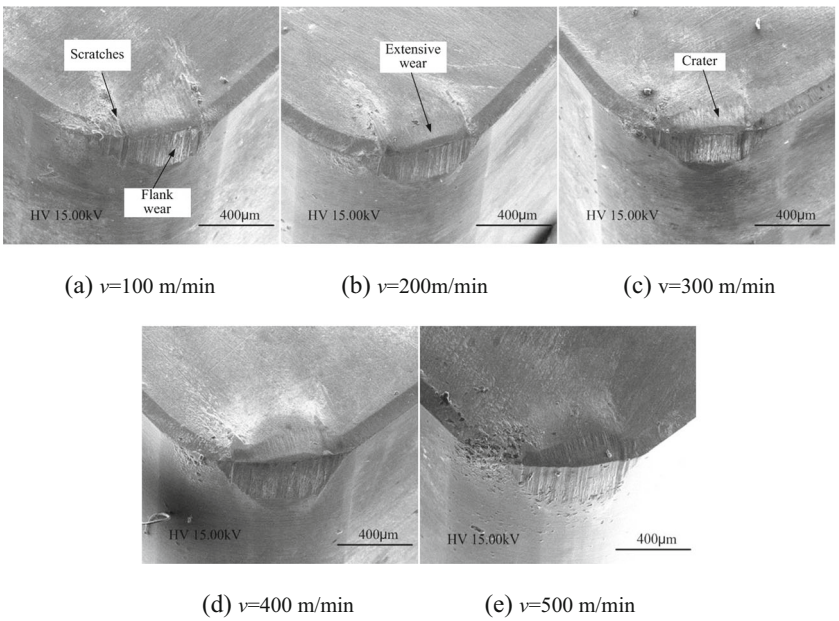

(a) v=100 m/min (b) v=200m/min (c) v=300 m/min

(d) v=400 m/min (e) v=500 m/min

Fig. 3 SEM of the worn CC650 ceramic tools in turning of ultra-high-strength steel 300 M at f = 0.1 mm/r and a_p = 0.1 mm

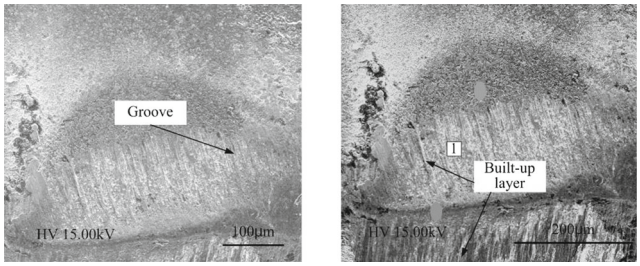

(a) Rake face (b) Flank face

Fig. 4 SEM micrographs of wear morphology on rake face and flank face of AT10N20 ceramic tools at $f = 0.1$ mm/r, $a_p = 0.1$ mm, and $v = 400$ m/min

and flank face also can be observed. This wear morphology is typical characteristic of abrasion and adhesion.

When turning ultra-high-strength steel 300 M at the lower cutting speeds, the dominance of wear mechanism was abrasion. With the increase of cutting speed, the cutting temperature also raised gradually, and the adhesion and the abrasion simultaneously occurred on both rake face and flank face. The crater wear on the rake faces (see Figs. 2d and 3c) resulted from interactions between the adhesion and the abrasion. With the further raise of cutting temperature, the soften effect could act on the workpiece due to the cutting heat generated in the high cutting process and the main wear mechanism will change to the adhesion gradually.

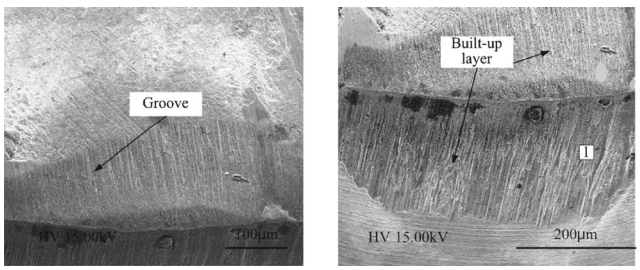

(a) Rake face (b) Flank face

Fig. 5 SEM micrographs of wear morphology on rake face and flank face of CC650 ceramic tools at $f = 0.1$ mm/r, $a_p = 0.1$ mm, and $v = 400$ m/min

Figure 6 shows the EDS analyses of worn surfaces for the AT10N20 and the CC650 ceramic cutting tools after machining at 300 m/min, respectively. It is seen from Fig. 4b that tool face at point 3 is much enriched with O, C, Al, Ti, and Fe elements. The O, C, Al, and Ti are mainly from Al_2O_3-based ceramic tool materials, while the Fe is the main element of ultra-high-strength steel 300 M. This analyses result showed that the adhesive wear occurred on the flank face of the AT10N20 ceramic tool. Point 1 in Fig. 5b is also much enriched the Fe element from ultra-high-strength steel, which is the evidence of adhesion of CC650 ceramic tool material.

At the initial and the steady wear stages, the adhering layers covered on the rake face and flank face of cutting tools, and reduced the deterioration of pits and grooves during machining process; hence the adhering layers protected ceramic tools from scratching action from hard particles, which could improve the tool life. At the rapid wear stage, some elements of the workpiece materials which could diffuse into to the ceramic tool caused the affinity between the workpiece materials and tool materials, and finally accelerated the tool wear rate. In addition, the low melting point of Fe element of workpiece materials could reduce the surface hardness of the ceramic tool. This could also accelerate the tool wear rate.

4 Conclusions

An Al_2O_3/TiC/TiN micro-nano-composite ceramic tool material (denoted as AT10N20) was hot pressed by adding 10 vol% nanoscale TiC, 10 vol% micro-scale TiC, and 20 vol% micro-scale TiN particles into the micro-scale Al_2O_3 matrix. The wear modes and wear mechanisms of the Al_2O_3/TiC/TiN ceramic cutting tools were investigated via turning of ultra-high-strength steel 300 M in comparison with those of Al_2O_3/TiC ceramic tool CC650. The following conclusions can be deduced from the findings of this study.

Fig. 6 EDS analyses for worn surface of AT10N20 and CC650 ceramic tools

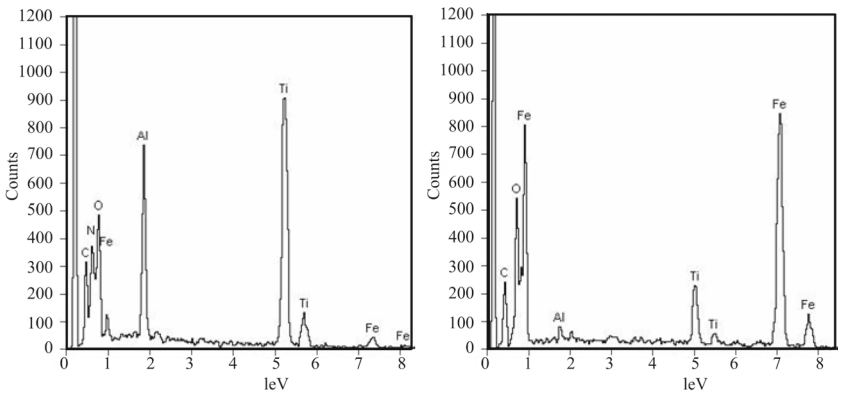

(a) Point 1 in Fig. 4b (b) Point 1 in Fig. 5b

1. Wear modes of AT10N20 and CC650 ceramic tools in turning of ultra-high-strength steel 300 M were flank wear and rake wear. At the lower cutting speeds, the dominant wear mode was flank wear and the slight scratches were found on the rake faces. With increase of the cutting speed, the rake wears became serious; in addition, the extensive crater wear on the rake faces and nose wear were clearly found.
2. Owing to crater wear on the rake face of AT10N20 initially occurred at cutting speed of 400 m/min, while that of the CC650 occurred at cutting speed of 200 m/min. In addition, the crater wear on the rake faces and flank wear was more severe when cutting speed was 400 m/min which was unfavorable for cutting of ultra-high-strength steel 300 M.
3. Wear mechanisms of AT10N20 and CC650 ceramic tools sliding against the ultra-high-strength steels involved abrasion, plastic flow, adhesion, and material transfer. When at the lower cutting speed, the domain of wear mechanism was abrasion. With the increase of cutting speed, the adhesion and the abrasion simultaneously occurred on both of rake face and flank face. With the further raise of cutting temperature, the main wear mechanism gradually changed to the adhesion.

Acknowledgments This work is sponsored by the National Natural Science Foundation of China (51475273), Shaanxi Science and Technology Research and Development Projects (2012 K06-19) and President Found of Xi'an Technological University (XAGDXJJ15005).

References

1. Bobbili R, Madhu V, Gogia AK (2013) Effect of wire-EDM machining parameters on surface roughness and material removal rate of high strength armor steel. Mater Manuf Process 28(4):364–368
2. Lipatov AA, Chigirinskii YL (2012) Performance of hard-alloy tools in turning high-strength martensitic steel. Russ Eng Res 32(3):285–287
3. Choudhury IA, El-Baradie MA (1998) Tool-life prediction model by design of experiments for turning high strength steel (290 BHN). J Mater Process Technol 77(1–3):319–326
4. Choudhury IA, El-Baradie MA (1997) Surface roughness prediction in the turning of high-strength steel by factorial design of experiments. J Mater Process Technol 67(1–3):55–61
5. Yang GY, Yu QX (1988) Tool life/cutting speed behavior in turning operations on high-strength steel. Werkstatt Betr Technol 121(5): 389–390
6. Abukhshim NA, Mativenga PT, Sheikh MA (2005) Investigation of heat partition in high speed turning of high strength alloy steel. Int J Mach Tools Manuf 45(15):1687–1695
7. Suresh R, Basavarajappa S, Gaitonde VN (2015) Experimental studies on the performance of multilayer coated carbide tool in hard turning of high strength low alloy steel. J Mater Res 30(20):3056–3064
8. Blinov EV, Blinov VM, Kostina MV, Bannykh OA (2008) Machinability of the high-strength corrosion-resistant high-ductility austenitic steel 06Kh22AG15N8M2F. Russ Metall 2008(2):128–132
9. Jiao L, Li T, Wang XB, Qin L, Chen JJ (2013) Wear mechanism of coated carbide insert in turning of low alloy ultra-high strength steel 35CrMnSi. Beijing Ligong Daxue Xuebao 33(1):22–25+36
10. Ashraf J, Olajire Kabiru A (1999) Turning of high strength steel alloy with PVD- and CVD-coated inserts. ASTM Spec Tech Publ 1362:71–85
11. Zheng GM, Zhao J, Gao ZJ, Cao QY (2012) Cutting performance and wear mechanisms of Sialon-Si3N4 graded nano-composite ceramic cutting tools. Int J Adv Manuf Technol 58:19–28
12. Zhao J, Yuan XL, Zhou YH (2010) Cutting performance and failure mechanisms of an Al_2O_3/WC/TiC micro- nano-composite ceramic tool. Int J Refract Met Hard Mater 28(3):330–337
13. Wang D, Zhao J, Chen XX, Zhou YH (2014) Wear mechanisms of ceramic tools in high-speed turning of superalloy GH2132. Key Eng Mater 589–590:23–27
14. Tian XH, Zhao J, Zhao JB, Gong ZC, Dong Y (2013) Effect of cutting speed on cutting forces and wear mechanisms in high-speed face milling of Inconel 718 with Sialon ceramic tools. Int J Adv Manuf Technol 69(9–12):2669–2678
15. Xu CH, Feng YM, Zhang RB, Zhao SK, Xiao X, Yu GT (2009) Wear behavior of Al2O3/Ti(C, N)/SiC new ceramic tool material when machining tool steel and cast iron. J Mater Process Technol 209(10):4633–4637
16. Grzesik W (2009) Wear development on wiper Al_2O_3-TiC mixed ceramic tools in hard machining of high strength steel. Wear 266(9–10):1021–1028
17. Yan LT, Yuan SM, Liu Q (2010) Cutting tool wear in the machining of hardened steels Part I: alumina/TiC cutting tool wear. Jixie Gongcheng Xuebao 46(9):187–192
18. Long ZH, Zhao WX, Dong SH (2008) Tribological property of high-strength steel work-piece subject to high speed machining strengthening (HSMS) surface modification. Mocaxue Xuebao 28(6):512–516
19. Barry J, Byrne G (2001) Tool wear and chip formation in green machining of high strength steel. Wear 247(2):139–151
20. Wang HX, Zong WJ, Liang YC, Dong S (2004) Tool geometry effect on machined surface integrity in precision turning high-strength spring steel. Mater Sci Forum 471–472:380–384